Journal of Power Sources 196 (2011) 1569–1577

Contents lists available at ScienceDirect

Journal of Power Sources

journal homepage: www.elsevier.com/locate/jpowsour

Structural transformation and its effects on the electrochemical performances of a layered double hydroxide

Meng Hu, Zhiyu Yang, Lixu Lei*, Yueming Sun

School of Chemistry and Chemical Engineering, Southeast University, Nanjing 211189, China

ARTICLE INFO

Article history:
Received 2 June 2010
Received in revised form 13 August 2010
Accepted 17 August 2010
Available online 24 August 2010

Keywords:
Ni–Al layered double hydroxide (LDH)
Stability
High temperature
Rare metal oxide
Alkaline secondary battery

ABSTRACT

When a layered double hydroxide (LDH), $[Ni_4Al(OH)_{10}]NO_3$ is aged at 60 °C in a concentrated KOH solution (around 7 mol L^{-1}), it transforms into β-$Ni(OH)_2$; when it is cycled electrochemically, it can also transform into β-$Ni(OH)_2$ but finish much sooner. In the mixture formed during the transformation, the reciprocal of the mass of the LDH is linearly related to the aging time. The electrochemical characterization of the LDH shows that the transformation impairs its performances, which leads to the decrease of the maximal number of exchanged electron per nickel atom as the charging/discharging cycling is continued. Therefore, this study reveals that the structural stability of the material, which is a key to its cycle life, depends on temperature, electrolyte concentration and electrochemical cycles. It was found that high temperature cyclic performances of the LDH can be improved by lowering the concentration of electrolyte and/or adding Lu_2O_3.

1. Introduction

Either pure or hybrid electric vehicles require their power supplying batteries to be reliable over a wide range of temperature; and the batteries certainly include nickel-based ones. As a candidate for the positive electrode materials for the nickel-based batteries, Ni–Al layered double hydroxide (LDH) [1–3], which can be represented by a general formula, $[Ni_xAl_y(OH)_{2(x+y)}]^{y+}A^{n-}{}_{y/n}\cdot mH_2O$ [1] (x, y, m and n are numbers determined by the stoichiometric composition of the compound; A^{n-} is the interlayer ions), has attracted many researchers for its stability in alkali solution around room temperature and advantageous electrochemical performances. For examples, no β-$Ni(OH)_2$ was detected after the material had been aged for 48 days at 22 °C [4] or 40 °C [1] and after hundreds of charge/discharge cycles at a rate of 0.2 C [4–6], 1.0 C [7] and even higher [8]. It can discharge a capacity of more than 300 mAh g^{-1} and be suggested as one of the lightweight electrode materials [4,7–10].

However, one thing must be considered for the cycle life of the Ni–Al LDH. Generally, a concentrated alkaline electrolyte is used for alkaline secondary batteries, and the Al^{3+} ions can be readily dissolved into the alkaline electrolyte in forms of $Al(OH)_4^-$ or its dehydrated form, AlO_2^- ions. Therefore, it is possible that Al^{3+} in the brucite-type layers may be leached out and enters into the solution. It is well known that LDHs lose their stability without the presence of trivalent cations [11,12]. In fact, it has been reported that with the absence of the trivalent cations, pure α-$Ni(OH)_2$ of a LDH structure readily transforms into β-$Ni(OH)_2$ in KOH electrolyte [13–15]; and there was also a report that Ni–Al LDH film can form β-$Ni(OH)_2$ with lost of Al^{3+} during repeating voltammetric scans in 0.1 mol L^{-1} NaOH [16]. Since β-$Ni(OH)_2$ is a worse electrode material than the Ni–Al LDH [1,8], the leaching out of Al^{3+} may degrade the electrode and thus influence its electrochemical performances. We have reported the particle size as well as the discharge capacity of the material shrinks and the material surface along with the electrode becomes coarser and coarser as the cycle number grows up [8]. It is possible that such morphological transformations serve as a prelude to the transformation reaction. Therefore, it is important to find when the transformation takes place and how to slow down the transformation rate.

In our previous studies [8], we observed that the $[Ni_4Al(OH)_{10}]OH$ electrode could be activated faster when the temperature of the electrolyte was elevated and behaves better than β-$Ni(OH)_2$ electrode. One of the reasons can be that the accelerated movement of ions and molecules makes the electrode be thoroughly wetted faster; we also observed that the discharged capacity of the LDH electrode decreases much faster than that of β-$Ni(OH)_2$ at high temperatures. Could this be caused by the lost of Al^{3+}? This paper reports our researches on the issue.

2. Experimental

2.1. Synthesis of $[Ni_4Al(OH)_{10}]NO_3$ and β-$Ni(OH)_2$

The starting LDH was prepared following the details in our previous paper [8], and it was dried to a constant weight at 90 °C

* Corresponding author. Tel.: +86 25 5209 0620x6421; fax: +86 25 5209 0618.
E-mail address: lixu.lei@seu.edu.cn (L. Lei).

0378-7753/$ – see front matter © 2010 Elsevier B.V. All rights reserved.
doi:10.1016/j.jpowsour.2010.08.041

Table 1
Stoichiometric formula and elemental analysis data of the samples.

Sample	Stoichiometric formula	Elemental analysis	
		Observed	Calculated
$[Ni_4Al(OH)_{10}]NO_3$	$[Ni_{3.9}Al(OH)_{9.8}]NO_3{\cdot}2H_2O$	Ni 44.0; Al 5.15; N 2.71; C 0.03; H 2.84	Ni 43.9; Al 5.18; N 2.69; C 0; H 2.67
1 day	$Ni_{4.2}Al(OH)_{10.4}(NO_3)_{0.2}(CO_3)_{0.4}{\cdot}3H_2O$	Ni 44.8; Al 4.86; N 0.51; C 1.08; H 2.94	Ni 45.6; Al 4.99; N 0.52; C 0.89; H 3.06
32 days	$Ni_{4.7}Al(OH)_{11.4}(NO_3)_{0.04}(CO_3)_{0.48}{\cdot}3H_2O$	Ni 46.7; Al 4.58; N 0.09; C 0.89; H 2.70	Ni 47.4; Al 4.64; N 0.10; C 0.99; H 3.01
105 days	$Ni_{6.1}Al(OH)_{14.2}(CO_3)_{0.5}{\cdot}4H_2O$	Ni 48.2; Al 3.62; N 0; C 0.79; H 2.57	Ni 49.1; Al 3.70; N 0; C 0.80; H 3.07
215 days*	$Ni_{6.6}Al(OH)_{15.2}(CO_3)_{0.5}{\cdot}2H_2O$	Ni 52.9; Al 3.69; N 0; C 0.72; H 2.42	Ni 52.4; Al 3.65; N 0; C 0.81; H 2.62
215 days	$Ni_{8.3}Al(OH)_{18.6}(CO_3)_{0.5}{\cdot}H_2O$	Ni 55.9; Al 3.18; N 0; C 0.51; H 2.27	Ni 55.5; Al 3.07; N 0; C 0.68; H 2.36
β-$Ni(OH)_2$	$Ni(OH)_{1.96}(CO_3)_{0.02}$	N 0; C 0.27; H 2.20	N 0; C 0.26; H 2.12

The sample with a star (*) was that aged at 60 °C for 105 days and continued to be aged at 10 °C for another 110 days.

before use. β-$Ni(OH)_2$ was also prepared as a reference by the same method with no addition of $Al(NO_3)_3$.

2.2. Studies on the stability of $[Ni_4Al(OH)_{10}]NO_3$ in an alkali solution

0.5000 g of $[Ni_4Al(OH)_{10}]NO_3$ was added into a 16 mL KOH solution (7 mol L^{-1}) in a 20 mL autoclave lined with Teflon. The autoclave was then placed into an oven maintained at 60 °C for 1, 4, 32, 105 or 215 days, and then the suspension was filtered with a 30 mL sintered glass funnel that was thoroughly washed and dried at 90 °C to a constant weight previously. The solid was washed with water and acetone several times, and then dried together with the funnel at 90 °C to a constant weight, from which the weight of the solid was determined by subtracting the weight of the funnel. The solid was then sampled for elemental analyses and electrochemical measurements, and it will be called as aged sample hereafter to distinguish it from the original sample.

2.3. Electrochemical characterization

50 mg of $[Ni_4Al(OH)_{10}]NO_3$ or the aged samples was thoroughly ground with 40 mg of natural flake graphite powder, several drops of 60 wt% polytetrafluoroethylene (PTFE) suspension to make a paste, and then inserted into a round sheet (15 mm in diameter) of nickel foam (Changsha, China, 1.6 mm thick, 425 g m^{-2}). The prepared electrode was dried at 90 °C for 24 h, pressed at 10 MPa for 1 min. The thickness of the disk was 0.5 mm in the end. We also employed 200 mg of metal nickel powder (200-mesh) in place of graphite for another cycling capacity test of the electrode. In the subsequent studies in this paper, we added 10 mg of rare earth metal oxides to investigate the effects on the high temperature performance of the electrode.

All electrochemical tests were done in a three-compartment electrolysis cell that contains a working electrode, a nickel plate counter electrode, and Hg/HgO reference electrode. Cyclic voltammetry (CV) diagrams were measured after 1 and 3 charge/discharge cycles using a CHI660b (Shanghai, China) electrochemical workstation at a scan rate of 0.1 mV s^{-1} from 0.15 V to 0.65 V. After immersed in 7 mol L^{-1} KOH at 60 °C for 1 h, the electrode was then cycled at a charge/discharge current density of 800 mA g^{-1} (charged for 30 min and discharged until the potential is 0 V vs. Hg/HgO). In this paper, current densities and discharge capacities per gram were all calculated according to the weight of the prepared materials.

2.4. Materials characterization

Analyses of metals were done with a J-A1100 ICP spectrometer; those of C, H, N were performed on a vario EL III elemental analyzer. FT-IR spectra were measured on a Nicolet 5700 in KBr disks. Powder X-ray diffractograms were recorded on a Rigaku D/MAX 2200 diffractometer using Cu Kα radiation (λ = 1.54056 Å). Scanning electron microscopy (SEM) was performed on a LEO1530VP scanning electron microscope. Transmission electron microscopy (TEM) was performed on a JEM2000EX transmission electron microscope.

Table 2
Diffraction data and calculated particle sizes in given directions for the samples.

Sample	LDH				β-$Ni(OH)_2$			
	Lattice parameters/Å		Crystalline size calculated by the diffraction of/nm		Lattice parameters/Å		Crystalline size calculated by the diffraction of/nm	
	a	*c*	(003)	(110)	*a*	*c*	(001)	(110)
$[Ni_4Al(OH)_{10}]NO_3$	3.06	23.74	21.9	28.5	–	–	–	–
1 day	3.05	23.59	21.4	27.6	3.09	4.56	7.1	18.4
32 days	3.04	23.24	19.4	20.5	3.09	4.60	11.2	21.1
105 days	3.04	23.25	23.6	20.0	3.09	4.60	11.7	20.9
215 days*	3.04	23.10	23.4	9.6	3.09	4.60	12.5	24.4
215 days	3.04	23.04	24.3	7.9	3.09	4.60	13.0	24.4
β-$Ni(OH)_2$	–	–	–	–	3.12	4.61	21.6	23.9

Note: The sample with a star (*) was that aged at 60 °C for 105 days and continued to be aged at 10 °C for another 110 days.

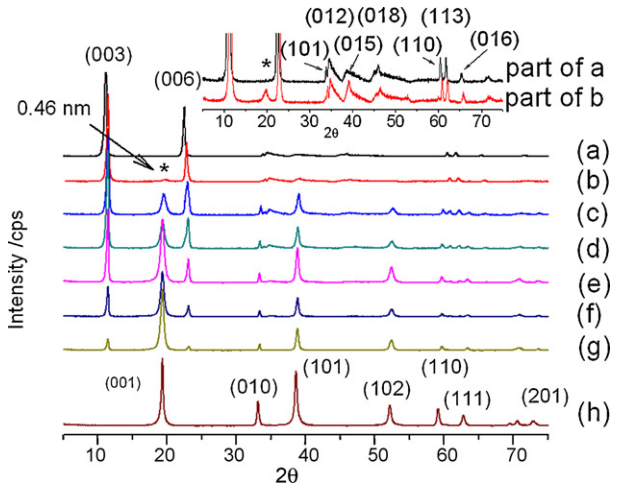

Fig. 1. XRD patterns of $[Ni_4Al(OH)_{10}]NO_3$ (a) original and aged at 60 °C in 7 mol L^{-1} KOH solution for (b) 1 day; (c) 4 days; (d) 32 days; (e) 105 days; (f) 105 days and then placed at 10 °C for another 110 days, (g) 215 days. That of β-$Ni(OH)_2$ is also shown in (h) for comparison. The star (*) shows that the (0 0 1) diffraction of β-$Ni(OH)_2$ (0.46 nm) appears after the LDH was aged for 1 day. The inset is the enlarged parts of curves of a and b.

3. Results and discussion

3.1. Transformation reaction of $[Ni_4Al(OH)_{10}]NO_3$ in alkali solution at 60 °C

All the XRD patterns of the $[Ni_4Al(OH)_{10}]NO_3$ samples are shown in Fig. 1, and their elemental analyses are shown in Table 1. It can be seen that the original $[Ni_4Al(OH)_{10}]NO_3$ has a stoichiometric formula of $[Ni_{3.9}Al(OH)_{9.8}]NO_3{\cdot}2H_2O$, which is slightly departed from the ideal composition, and its XRD pattern is similar to those previously reported by us [8–10]. After being treated in alkali solution for 1 day, the (0 0 3) reflection of the XRD pattern shifts to a higher 2θ value (Fig. 1a and b). It should be reminded that CO_3^{2-} always exists in KOH, and CO_3^{2-} is more competitive than OH^-, NO_3^- [17], therefore, some of the compounds contain CO_3^{2-}. As the aging time extends, β-$Ni(OH)_2$ appears and grows.

The LDH phase in all the samples can be indexed on a rhombohedral cell of space group $R\bar{3}M$, the c parameter changes from 23.74 Å to 23.04 Å as the aging time extends (Table 2), which may be attributed to the anion exchange. It has been reported that the basal spacing corresponding to c value depends on the compositions of Ni^{2+} and Al^{3+} ions and the maximum occurs when the molar ratio of Ni to Al is about 4:1 [4,18]. The loss of Al^{3+} is unambiguous from Table 1, in which the molar ratio of Ni to Al changes from 3.9:1 of the original to 8.3:1 after 215 days. The a parameter also decreases a little from 3.06 Å to 3.04 Å as the aluminum content decreases, which may be attributed to the loss of Al^{3+} ions. It was also observed that concentration of Al^{3+} lowered as a Ni–Al LDH film electrode was potentially cycled in 0.1 mol L^{-1} NaOH [16].

In Fig. 1, it can be seen that β-$Ni(OH)_2$ appeared after the original sample was treated for 1 day, and it grew and exceeded the LDH in 105 days assuming that the intensity of the corresponding signals are equally representative of the amount of each compound in the mixture. The diffractions belong to β-$Ni(OH)_2$ can be indexed on a hexagonal cell with space group of $P\bar{3}M1$. The c and a values are consistent with the literature values [19–23] and the synthesized reference, β-$Ni(OH)_2$ in this paper (Table 2). Compared with the report which employed Ni–Al LDH with Cl^- as interlayer anion [16], this work does not show any other new phases.

According to the Scherer equation, the crystalline size for LDH estimated by the (0 0 3) reflection grows a little (about 3.0 nm), but that estimated by the (1 1 0) reflection reduces greatly (about 20 nm); for β-$Ni(OH)_2$ the crystalline sizes estimated by both (0 0 1) and (1 1 0) reflections increase (Table 2). This means that the LDH becomes smaller but thicker, and the β-$Ni(OH)_2$ becomes bigger and bigger.

Fig. 2 shows the IR spectra of the samples. There is a band at 1365 cm^{-1} attributed to the vibration of CO_3^{2-} [24] in the samples aged for 32 days and 215 days (Fig. 2b), therefore, CO_3^{2-} intercalates into the interlayer space of LDH by an anion-exchange process. As it is known, carbonate formed by the base absorbing CO_2 from ambient air cannot be excluded fully in LDH chemistry. It is very interesting that the intensity and area of the two bands at 1365 cm^{-1} and 1380 cm^{-1} (from both the vibrations of CO_3^{2-} and NO_3^{2-}) decrease as the aging time goes. Also, a sharp peak centered at 3640 cm^{-1} due to non-hydrogen bonded hydroxyl groups in β-$Ni(OH)_2$ [25,26] appears for the sample aged for 32 days and intensifies for the sample aged for 215 days, and the intense broad absorption band in the range of 3400 cm^{-1} and 3600 cm^{-1} corresponding to the stretching vibrations of the hydroxyl groups of interlayer and absorbing water molecules [2] becomes smaller and smaller, indicating the loss of water molecules (Fig. 2a). Therefore, both the anions are excluded from the materials as the aging process goes, and the transformation of LDH into β-$Ni(OH)_2$ as indicated by the XRD patterns occurs. This is also supported by the elemental analyses in Table 1.

The mass of the $[Ni_4Al(OH)_{10}]NO_3$ was measured after being soaked in 7 mol L^{-1} KOH at 60 °C for certain days, and the results are shown in Table 3. It can be seen that the mass decreases continuously. Suppose that the leaching reaction of Al^{3+} causes $[Ni_4Al(OH)_{10}]NO_3$ to decompose, and only β-$Ni(OH)_2$ remains in the solid:

$$[Ni_{3.9}Al(OH)_{9.8}]NO_3{\cdot}2H_2O + 2OH^-$$

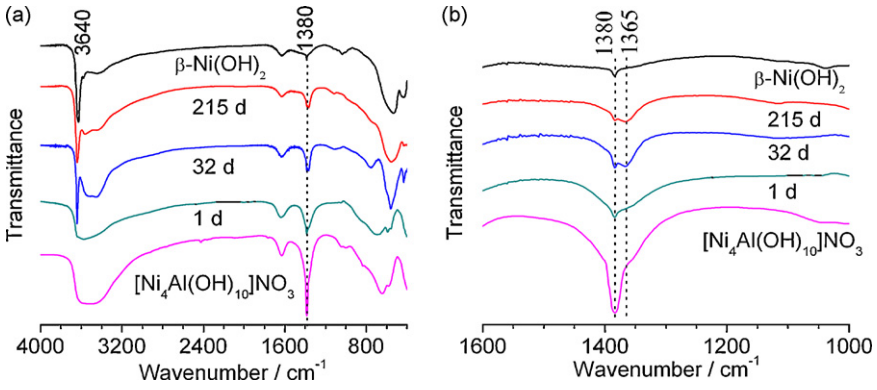

Fig. 2. FT-IR spectra between (a) 400 and 4000 cm^{-1}; (b) 1000 and 1600 cm^{-1} of the origin $[Ni_4Al(OH)_{10}]NO_3$ and the samples aged for 1 day; 32 days; 215 days and β-$Ni(OH)_2$.

Table 3
Mass and concentration data in the aged samples.

Sample	m_{obsd}/g	m_{LDH}/g	m_{β}/g	x_{LDH}/%	$((1/m_{LDH})-(1/m_0))$/g^{-1}
1 day	0.4722	0.4090	0.0632	100	0.4451
32 days	0.4459	0.3229	0.1230	86.6	1.0972
105 days	0.4108	0.2080	0.2028	72.4	2.8088
215 days	0.3896	0.1385	0.2510	50.6	5.2180

Note: m_{obsd} is the residual mass of the rest solid mixture after aged; m_{LDH} and m_{β} are the calculated values according to Eq. (1) and m_0 is the original mass i.e. 0.5000 g. x_{LDH} is the mass percentage of the $[Ni_4Al(OH)_{10}]NO_3$ LDH in the active material.

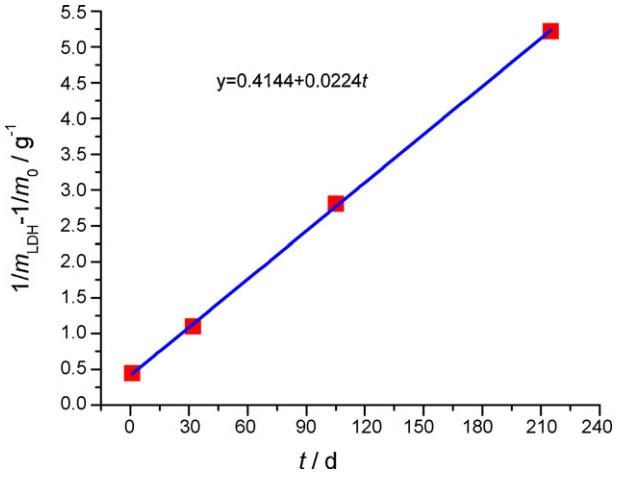

Fig. 3. A plot of $((1/m_{LDH})-(1/m_0))$ against t (the aging time). m_{LDH} refers to the residual mass of LDH in the aged sample and m_0 is the mass before the aging, which is 0.5000 g.

$$= 3.9\beta\text{-}Ni(OH)_2 + Al(OH)_4^- + NO_3^- + 2H_2O \quad (1)$$

Then the total mass can be decomposed into two parts according to the molar ratio of Ni to Al. For example, if the Ni/Al ratio is found to be 4.2:1, there are 0.3 mole of β-$Ni(OH)_2$ and 1 mole of $[Ni_{3.9}Al(OH)_{9.8}]NO_3{\cdot}2H_2O$. By this way, we get the values in Table 3. A plot of $((1/m_{LDH})-(1/m_0))$ against t (the aging time) shows a straight line (Fig. 3), which means the transformation reaction obeys a second-order reaction law [27].

3.2. Morphological changes

Fig. 4 shows SEM images of the $[Ni_4Al(OH)_{10}]NO_3$ LDH and the samples aged in alkali solution and Fig. 5 shows their TEM images. Similar to other reports [28–30], the $[Ni_4Al(OH)_{10}]NO_3$ LDH contains piles of well-developed disks with round vertexes as shown by both SEM and TEM (Figs. 4 and 5a). However, all the aged samples are composed of regular hexagonal disks with diameters from 40 nm to 800 nm (Figs. 4b–d and 5b). The thickness of the disks in all samples varies from 15 to 100 nm (Figs. 4 and 5). The size of the disks changes unlike what the Scherer equation predicts, but it can be seen there are both very small and very big disks, and the Scherer equation calculates the average.

Fig. 5 also shows variations of the selected-area electron diffraction (SAED) patterns obtained from TEM samples. The $[Ni_4Al(OH)_{10}]NO_3$ LDH at the beginning shows two diffraction rings of the hexagonal packed structure and the spots on the rings show obvious sixfold symmetry, which is similar to the reported SAED results [31] but after indexed on a hexagonal cell, a and c can be calculated as 3.04 ± 0.02 Å and 24.5 ± 1.0 Å by the basal spacing (shown in Fig. 5, $d_{0\,1\,2} = 2.60$ Å, $d_{1\,1\,0} = 1.53$ Å; the constant of the TEM was 35.8 mm Å), which are very close to the results listed in Table 2. As the LDH transforms into β-$Ni(OH)_2$, the diffraction rings evolves into spots. The spots in the SAED pattern appear more and more clearly as the aging time goes, and after the sample has been aged for 215 days, the rings disappear completely. Therefore, the crystallinity of the product becomes better and better. The diffraction spots can be indexed on a hexagonal cell. The spots with d values, 2.70 Å and 1.56 Å correspond to the diffraction of (0 1 0) and (1 1 0) crystal planes of β-$Ni(OH)_2$, and the calculated a is 3.12 ± 0.02 Å. In addition, it is also found that the surface of disks becomes coarser and coarser, and some bright spots and irregular lines appear later on the disks as the aging time goes (Fig. 5c and d). This is similar to our previous results for the electrode material after many charge/discharge cycles [8].

These morphological changes may indicate that left Al^{3+} ions cause some strain in the lattice. Because $Ni(OH)_2$ has limited solubility in water, it is reasonable to suggest that β-$Ni(OH)_2$ grows up directly from the remains of $[Ni_4Al(OH)_{10}]NO_3$. Therefore, there are both β-$Ni(OH)_2$ and LDH in the aged samples (Fig. 5).

3.3. Phase transformation at a lower temperature

Now that the phase transformation is definite to take place at 60 °C, we are eager to know the details of the transformation at a lower temperature. We take a autoclave out after it had been kept in an oven maintained at 60 °C for 105 days and place it at a surroundings temperature of 10 °C for another 110 days. Elemental analysis of the sample (Table 1) shows that the calculated atom ratio of Ni to Al is 6.6, which is between 6.1 for the sample aged

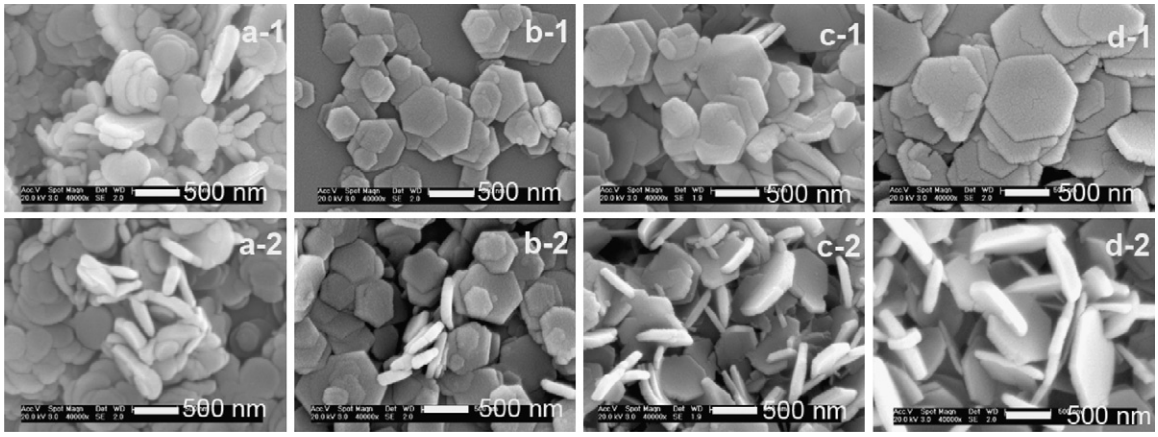

Fig. 4. SEM images of (a) the $[Ni_4Al(OH)_{10}]NO_3$ LDH and the sample aged for (b) 1 day; (c) 32 days and (d) 215 days.

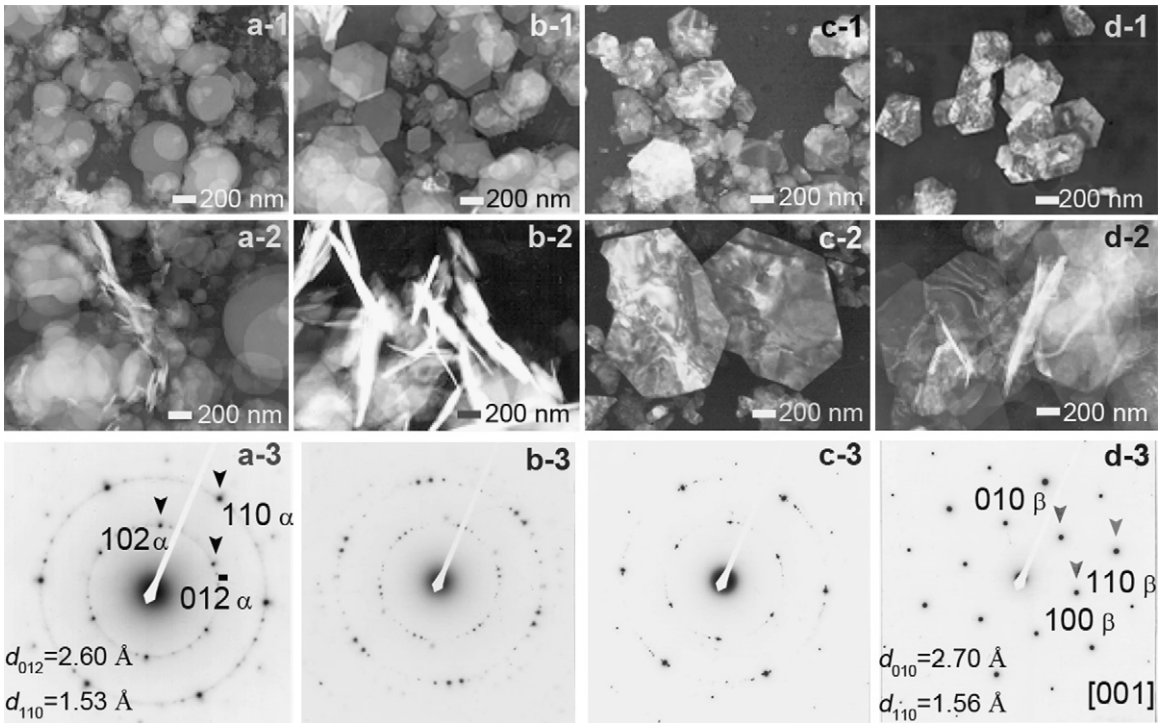

Fig. 5. TEM images of (a) the $[Ni_4Al(OH)_{10}]NO_3$ LDH and the sample aged for (b) 1 day; (c) 32 days and (d) 215 days. The corresponding SAED patterns were obtained from the hexagonal disks randomly selected in the samples.

for 105 days and 8.3 for the sample aged for 215 days at 60 °C. The XRD pattern also indicates the intensity of β-$Ni(OH)_2$ reflections intensified and that of LDH reflections reduced (Fig. 1). Therefore, we conclude that the transformation from LDH phase to β-$Ni(OH)_2$ can take place but becomes more slowly at a temperature as low as 10 °C. This is likely in conflict with many results which reported the LDH material is quite stable because no β-$Ni(OH)_2$ was detected after it was aged for a long time at room temperatures such as at 22 °C [4] or 40 °C [1]. We believe that there are two possibilities that lead to the results. One is that the reaction is very slow at lower temperatures, therefore, more time should be needed to have such observations; the other is, there is no highly crystallized β-$Ni(OH)_2$, which is desperately required by XRD detections.

3.4. Phase transformation during the charge–discharge cycles at different temperatures

In order to observe the transformation of the active material during the charge–discharge cycles, after the electrode had been charged and discharged for 1, 2, 3, 5, 12, 26 and 130 cycles at 60 °C respectively, it was washed with water for several times, dried at 60 °C under vacuum condition and then detected by XRD. Fig. 6 shows XRD patterns of the $[Ni_4Al(OH)_{10}]NO_3$ obtained from the electrode after the 1st, 2nd, 3rd, 5th, 12th, 26th and 130th charge/discharging cycles at 60 °C respectively, in comparison with the freshly prepared electrode and the electrode after soaked in alkali solution for 1 h at the same temperature. The LDH material in the freshly prepared electrode has a *d* value of 7.90 Å and a calculated particle size of 21.5 nm in (0 0 3) crystallite direction (Table 4). Therefore, there is no change in structure during the preparation of the electrode (please refer to Table 2). After the electrode was soaked in the alkali solution, the *d* value and size of the active material decrease, which are 7.74 Å and 19.1 nm, respectively. Later, both of them decrease as the cycle number grows up, which are 7.54 Å and 9.86 nm respectively after 12 cycles. It is only 26 cycles that

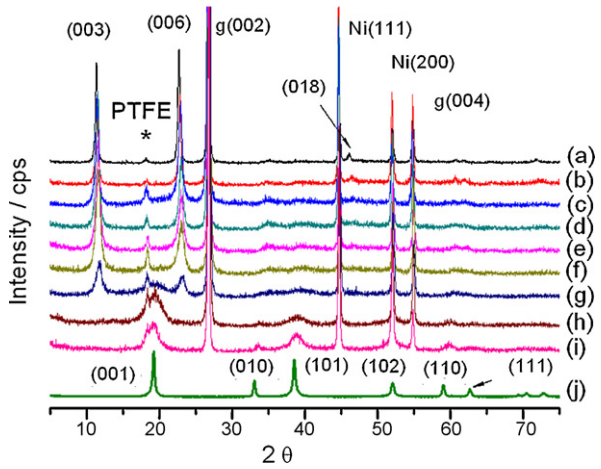

Fig. 6. XRD patterns of the $[Ni_4Al(OH)_{10}]NO_3$ electrode: (a) freshly prepared; (b) been soaked in 7 mol L^{-1} KOH solution at 60 °C for 1 h; been charged and discharged for (c) 1, (d) 2, (e) 3, (f) 5, (g) 12, (h) 26 and (i) 130 cycles, in comparison with that of (j) as-prepared β-$Ni(OH)_2$. The peak at about 18° with a star (*) is from PTFE, which is used as binder in the electrode. Peaks indicated with g(0 0 2), g(0 0 4), Ni(1 1 1) and Ni(2 0 0) are from graphite and nickel foam, respectively.

LDH can no longer be detected and a series of broadened peaks from β-$Ni(OH)_2$ as well as the peaks attributed to additives such as PTFE, graphite and the substrate nickel are left. After the 130th cycle, which takes only 4 days, the peaks of β-$Ni(OH)_2$ are clearly observed. Obviously, under the condition of electrochemical cycles, the transformation of LDH into β-$Ni(OH)_2$ at 60 °C proceeds more quickly, and due to the transformation, the discharge capacity of the active material drops significantly (Table 4).

Another similar investigation was carried out at 20 °C. An elemental analysis of the electrode material removed from the electrode after 277 cycles, which takes 9 days, shows that the calculated molar ratio of Ni to Al turns out to be 4.6. Since the active mate-

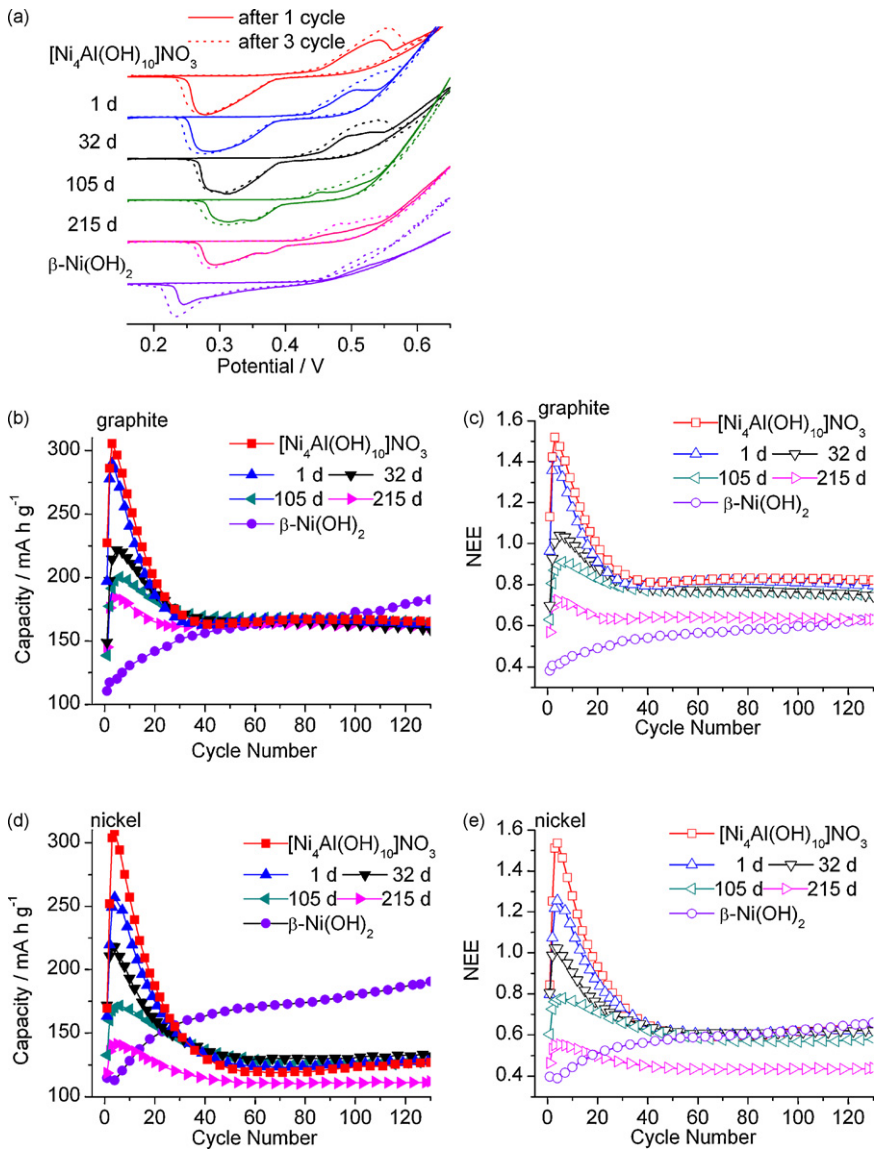

Fig. 7. (a) CV curves of the prepared electrodes at a scan rate of 0.1 mV s^{-1}; (b, d) the electrode capacity and (c, e) the number of exchanged electrons (NEE) vs. cycle number employing graphite and nickel powder as the conductive agent, respectively. The solid lines indicate the CV curves after the electrode was charged and discharged for 1 cycle and the dot lines indicate those for 3 cycles. All the measurements were taken at 60 °C.

rial may be contaminated by the substrate Ni foam, this result may be not very significant, it can only be concluded that the transformation proceeds much slower under such circumstances. No β-$Ni(OH)_2$ phase in the sample can be detected by XRD, which could be expected because the LDH material can keep its layered structure even though the ratio of Ni to Al is as high as 9.0 (10 mol%) [4,11], and also the β-$Ni(OH)_2$ formed is only in very small amount. And for the electrode cycled at high current densities, the conclusion

Table 4
The *d* values, calculated particle sizes of LDH and β-$Ni(OH)_2$ in the cycled electrodes with their corresponding discharge capacities.

Sample	LDH		β-$Ni(OH)_2$		Discharge capacity/mAh g^{-1}
	d value/Å	Crystalline size/nm	*d* value/Å	Crystalline size/nm	
Freshly prepared	7.90	21.5	–	–	–
Soaked for 1 h	7.74	19.1	–	–	–
Cycled for					
1	7.73	14.6			227.2
2	7.67	12.7	–	–	286.1
3	7.63	12.2	–	–	305.4
5	7.62	9.86	–	–	296.3
12	7.54	8.03	–	–	257.6
26	–	–	4.61	3.1	179.1
130	–	–	4.62	4.0	165.0

Notes: The crystalline sizes are calculated by the Scherer equation according to the (0 0 3) diffraction for LDH and the (0 0 1) diffraction for β-$Ni(OH)_2$.

should be about the same because the measurement lasted only 9 days for about 300 cycles in our previous paper [8], which is also much shorter than 2 months spent by the stability testing of this paper [4,11].

3.5. Effect of the transformation on the electrochemical behaviors

Table 4 shows that the discharge capacity which is 227.2 mAh g^{-1} at the 1st cycle, and the maximum 305.4 mAh g^{-1} at the 3rd cycle, decreases to 165 mAh g^{-1} at the 130th cycle with the transformation of the LDH to β-$Ni(OH)_2$. This rapid decreasing in the electrode capacity reminds us that such a transformation could play a key role in the electrochemical behaviors of the electrode, thus requires detailed inspection on the electrochemical behaviors of the materials.

Fig. 7a shows CV curves of $[Ni_4Al(OH)_{10}]NO_3$ and the aged active materials on the electrodes at a scan rate of 0.1 mV s^{-1} at 60 °C. For the $[Ni_4Al(OH)_{10}]NO_3$ electrode, the pair of redox peaks is much more symmetrical than the others, indicating a good electrochemical reversibility. However, as the LDH had been aged for days, the pairs of peaks become more and more asymmetric: the peaks are distorted and even split into several peaks. In contrast, β-$Ni(OH)_2$ has the most asymmetric peak pair in which the oxidation peak even dissolves into the curve of the oxygen evolution. Therefore, the above electrochemical responses may be attributed to the transformation of the LDH.

Fig. 7b–e shows the cycling performances of the active material using two different conducting agents, i.e. graphite or metallic nickel powder, respectively. When only nickel powder (200 mg) was employed as the conducting agent instead, similar results can be obtained although the electrode has a little worse electrochemical performance than the corresponding electrode using natural flake graphite (40 mg) as the conducting agent. Take the graphite electrode as an example, the capacity of the $[Ni_4Al(OH)_{10}]NO_3$ LDH electrode reaches its maximum of 305.4 mAh g^{-1} at the 3rd cycle, then drops to gradually and stabilizes at 179.1 mAh g^{-1} after the 26th cycle. The number of exchanged electrons (NEE) per nickel atom can be larger than 1.5. However, when the material is aged, the capacity of the material decreases greatly as the time lasts. For example, the capacity of the material aged for 215 days at the 1st cycle is 145.1 mAh g^{-1}, the maximum is 184.9 mAh g^{-1}, and the NEE is lower than 0.8. The capacity for β-$Ni(OH)_2$ increases the most slowly and cannot reach its maximum even after 130 cycles; the NEE never exceeds 1.0.

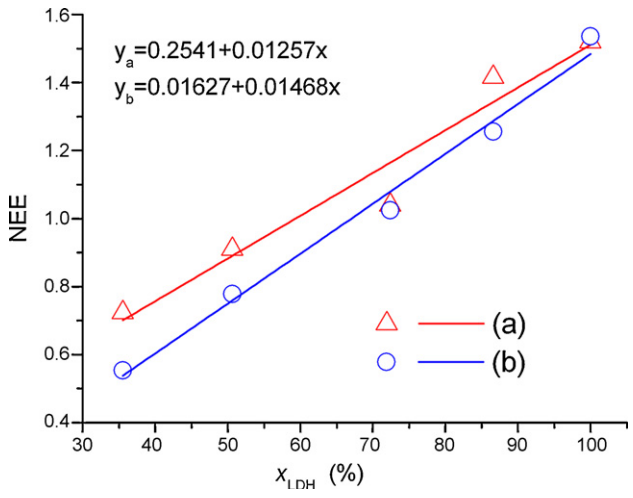

Fig. 8. Plots of the maximal NEE against x_{LDH} with (a) graphite; (b) nickel powder as the conducting agent. x_{LDH} is the mass percentage of the $[Ni_4Al(OH)_{10}]NO_3$ LDH in the active material. The data dots are linearly fitted.

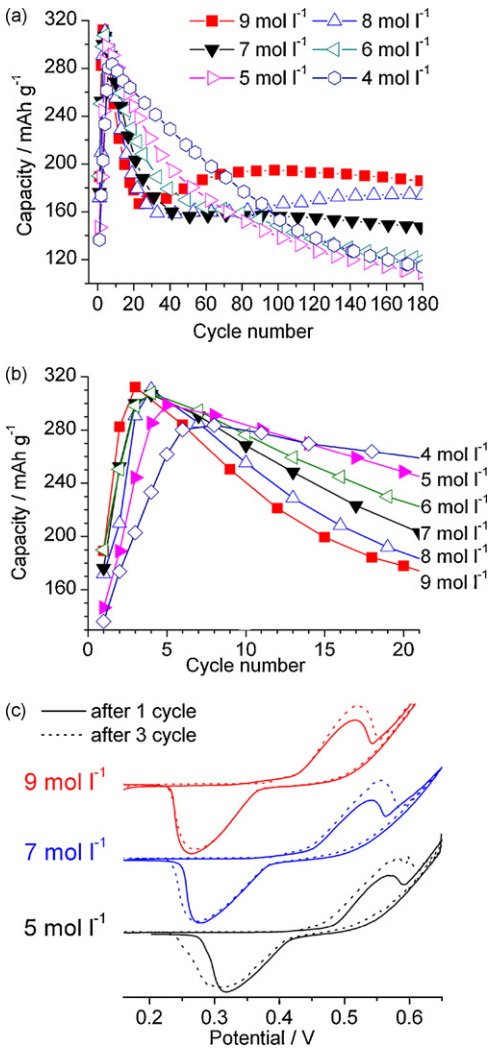

Fig. 9. (a) Capacity of the $[Ni_4Al(OH)_{10}]NO_3$ electrode vs. cycle number, (b) its enlarged part from 1 to 20 cycles; (c) CV curves in different concentrated KOH solution. The solid lines were obtained after the electrode was charged and discharged for 1 cycle and the dot lines for 3 cycles. All the curves were measured at 60 °C and all the electrodes employed natural flake graphite (40 mg) as the conducting agent.

Fig. 8 shows the plots of the maximal number of exchanged electrons (NEE) against the mass percentage of the $[Ni_4Al(OH)_{10}]NO_3$ LDH in the active material (x_{LDH}, data listed in Table 3). The NEE increases linearly with the portion of the LDH for both the conducting agents, therefore the transformation from LDH to β-$Ni(OH)_2$ results in the degradation of the electrode. It is well known that β-$Ni(OH)_2$ is a worse active material [14,32,33] than the LDH.

Fig. 7 also shows that all the discharge capacities of the electrode materials stabilize in 20 cycles. At that time, the transformation reaction almost ends according to the XRD patterns (Fig. 6), since no diffractions from LDH can be detected.

Therefore, it can be concluded that the LDH destabilizes at higher temperature, and it needs to be stabilized if we want to make use of it. In the following contexts we tried to change the electrolyte concentration and add some rare earth oxides in order to improve the performance of the electrode.

3.6. Effect of the electrolyte concentration

According to Eq. (1) and the electrode reaction, OH^- is a reactant that can influence the compositions of active materials in the electrodes; it is also a reactant of the electrode reaction and the

Table 5
Summary of the characteristics potentials of the electrodes at 60 °C.

Electrode	After 1 cycle						After 3 cycles					
	E_{pa}/mV	E_{pc}/mV	ΔE_p/mV	E_{rev}/mV	E_{OE}/mV	$E_{OE}-E_{pc}$/mV	E_{pa}/mV	E_{pc}/mV	ΔE_p/mV	E_{rev}/mV	E_{OE}/mV	$E_{OE}-E_{pc}$/mV
5 mol L^{-1} KOH	317	570	253	444	592	22	313	588	275	450	616	28
7 mol L^{-1} KOH	279	542	263	410	563	20	272	557	285	414	583	26
9 mol L^{-1} KOH	264	516	252	390	543	27	270	518	248	394	555	37
7 mol L^{-1} KOH, with												
Lu_2O_3	305	537	232	421	560	23	288	542	254	415	571	29
Er_2O_3	306	519	213	412	543	24	292	536	244	414	566	30
Y_2O_3	299	520	221	410	542	22	280	545	265	412	579	34
La_2O_3	277	540	263	408	563	23	272	557	285	414	585	28

Note: E_{pa} and E_{pc} is the oxidative and reductive potential; ΔE_p is the difference between E_{pc} and E_{pa}; E_{rev} is the average potential; E_{OE} for oxygen revolution potential; $E_{OE}-E_{pc}$ is the difference of the oxidative and oxygen revolution potential.

supporting electrolyte. Fig. 9a and b shows the charge/discharge behaviors of the $[Ni_4Al(OH)_{10}]NO_3$ electrode in KOH solution of different concentrations at 60 °C. As shown, the electrode can be more easily activated in a higher concentrated alkali solution. For example, in 9, 7 and 5 mol L^{-1} KOH solutions the first capacities of the electrodes are 189.3, 176.2, 146.7 mAh g^{-1}, respectively; their maximal capacities, 312.2, 306.7 and 298.9 mAh g^{-1} correspond to the cycle number is 3, 4 and 5, respectively. This is understandable because the electrode processes is diffusion-controlled [8], and higher concentration of electrolyte can promote the diffusion process from the electrolyte to the body of the electrode.

Fig. 9a also shows that the capacity of each electrode generally decreases as the cycle number increases, but it decreases more slowly in less-concentrated solutions. This may indicate that the transformation of the active material slows down as the concentration of alkali solution goes down. However, after some 80 cycles, the performance of the electrode becomes much worse in 4, 5 and 6 mol L^{-1} KOH than in 7 and 9 mol L^{-1} KOH (Fig. 9b). The reason for this phenomenon is not clear, but one reason may be the faster erosion of nickel foam at higher concentration of KOH at 60 °C, however, but it is not enough to elucidate the whole change.

Fig. 9c shows the CV curves for the electrode in the KOH solutions of different concentration and Table 5 lists their characteristic potentials. The electrode in 9 mol L^{-1} KOH has a smaller difference between the oxidative and reductive potential, ΔE_p and a larger difference between the oxygen evolution and the oxidation potential, $E_{OE}-E_{pc}$ than the other two in KOH at lower concentrations. In addition, the average potential which can be taken as an estimate of the reversible potential [34] are found to move toward the negative direction from 444 mV to 390 mV as the concentration of the alkali solution increases from 5 mol L^{-1} to 9 mol L^{-1} KOH. This means that KOH solution of higher concentration could produce less oxygen during charging, therefore leads to better electrode performance, while the electrode in less-concentrated alkali solutions has to suffer more impacts from oxygen evolution. The oxygen evolution will certainly loose the electric contact among the active material particles, thus worsen the performance of the electrodes. This could be another reason why the electrochemical performance improves after 80 cycles as the concentration of KOH increases (Fig. 9a and b).

3.7. Effects of rare earth oxide additives

It has been found that rare metal oxides are particularly effective to raise the high temperature charge acceptance of nickel electrodes [35–39], therefore, we would like to see if they works with our electrode material. Fig. 10a shows curves of the discharge capacities versus cycle number when some rare earth oxides were added to the electrode. The trend of curves is similar to each other, but addition of Lu_2O_3, Er_2O_3, Y_2O_3 and La_2O_3 make less and less positive effect on the performance of $[Ni_4Al(OH)_{10}]NO_3$ electrode. Generally, lanthanide oxides will turn out to be hydroxides in water, [40] and the hydroxides should cover the surface of the electrode material and may inhibit the dissolution of Al^{3+}. The solubility product, K_{sp} at 25 °C for $Lu(OH)_3$, $Er(OH)_3$, $Y(OH)_3$ and $La(OH)_3$ are 2.5×10^{-24}, 1.3×10^{-23}, 8.1×10^{-23} and 1.0×10^{-19}, respectively [41]. As the K_{sp} is getting bigger, the solubility of the hydroxides is getting bigger. Combined with sequence of positive effect on cyclic performance of lanthanide oxide additives, it may lead to a conclusion that the lanthanide hydroxide with smaller solubility leads to higher cyclic performance of $[Ni_4Al(OH)_{10}]NO_3$ electrode. This is just on the contrary of another system in which the utilization of $Ni(OH)_2$ active material with the addition of $Ca(OH)_2$, $Mg(OH)_2$, $Cd(OH)_2$, $Co(OH)_2$ and $Zn(OH)_2$ decreases according to the decreasing sequence of their solubility product [42].

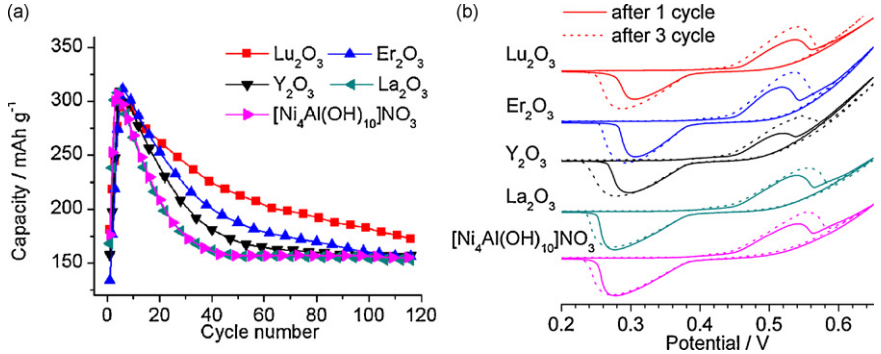

Fig. 10. (a) Capacity vs. cycle number; (b) CV curves at 60 °C after the electrode was added some rare earth oxides, respectively. The solid lines were obtained after the electrode was charged and discharged for 1 cycle and the dot lines for 3 cycles. All the curves were measured at 60 °C and the electrodes employed natural flake graphite (40 mg) as the conducting agent.

Fig. 10b shows the CV curves of the electrode with lanthanide oxide additives, and Table 5 also lists the characteristics potentials. Compared with the electrode without lanthanide oxide additives in the same concentration of electrolyte, their potential gaps, ΔE_p decrease greatly (20–50 mV s) except La_2O_3 being used as the additive, indicating that Lu, Er and Y oxides (hydroxides) make the electrode reaction more reversible; but the gaps, $E_{OE} - E_{pc}$ have only a little changes (2–4 mV s). This means that the reversibility of the redox reaction plays a more important role in the electrode performance.

4. Conclusions

When layered double hydroxide $[Ni_4Al(OH)_{10}]NO_3$ meets OH^- ions in the alkali electrolyte, two reactions will occur: (1) anion exchange of OH^- for $NO_3{}^-$; (2) loses some Al^{3+} and convert to β-$Ni(OH)_2$, because $Al(OH)_4{}^-$ is soluble in concentrated alkali solution. The second process can be observed both in the aging and the charge–discharge processes by the elemental analysis and XRD; and the reaction obeys a second-order reaction law.

The transformation from LDH to β-$Ni(OH)_2$ leads to a degradation of the electrodes, because the well-crystallized β-$Ni(OH)_2$ has a poor electrochemical activity. It is observed that the maximal number of exchanged electrons (NEE) of the electrodes increases as the amount of β-$Ni(OH)_2$ decreases in the composition of the electrode, using either nickel powder or graphite as the conducting agent.

The concentration of the electrolyte solution and the addition of rare metal oxides may affect the electrode performance. The results are: (1) the electrode in a less-concentrated solution degrades the electrode less slowly, but it has a better electrochemical performance in a more concentrated solution; (2) addition of Lu_2O_3, Er_2O_3 or Y_2O_3 to the electrode can slow down the degradation of electrode, but addition of La_2O_3 almost has no effects on the performance of electrode.

Acknowledgements

We would like to thank The Office of Personnel, Jiangsu Province and The Southeast University for financial supports.

References

[1] K.T. Ehlsissen, A. Delahaye-Vidal, P. Genin, M. Figlarz, P. Willmann, J. Mater. Chem. 3 (1993) 883–888.
[2] C. Li, L. Wang, M. Wei, D.G. Evans, X. Duan, J. Mater. Chem. 18 (2008) 2666–2672.
[3] G.R. Williams, D. O'Hare, J. Mater. Chem. 16 (2006) 3065–3074.
[4] W.K. Hu, D. Noreus, Chem. Mater. 15 (2003) 974–978.
[5] J.X. Dai, S.F.Y. Li, T.D. Xiao, D.M. Wang, D.E. Reisner, J. Power Sources 89 (2000) 40–45.
[6] C.Y. Wang, S. Zhong, K. Konstantinov, G. Walter, H.K. Liu, Solid State Ionics 148 (2002) 503–508.
[7] W.K. Hu, X.P. Gao, D. Noreus, T. Burchardt, N.K. Nakstad, J. Power Sources 160 (2006) 704–710.
[8] M. Hu, X. Gao, L. Lei, Y. Sun, J. Phys. Chem. C 113 (2009) 7448–7455.
[9] L. Lei, M. Hu, X. Gao, Y. Sun, Electrochim. Acta 54 (2008) 671–676.
[10] M. Hu, L.X. Lei, J. Solid State Electrochem. 11 (2007) 847–852.
[11] G.A. Caravaggio, C. Detellier, Z. Wronski, J. Mater. Chem. 11 (2001) 912–921.
[12] T. Pan, J.M. Wang, Y.L. Zhao, H. Chen, H.M. Xiao, J.Q. Zhang, Mater. Chem. Phys. 78 (2003) 711–718.
[13] A. Delahaye-Vidal, B. Beaudoin, N. Sac-Epee, K. Tekaia-Elhsissen, A. Audemer, M. Figlarz, Solid State Ionics 84 (1996) 239–248.
[14] P. Oliva, J. Leonardi, J.F. Laurent, C. Delmas, J.J. Braconnier, M. Figlarz, F. Fievet, A. de Guibert, J. Power Sources 8 (1982) 229–255.
[15] H. Bode, K. Dehmelt, J. Witte, Electrochim. Acta 11 (1966) 1079–1087.
[16] R. Roto, L. Yu, G. Villemure, J. Electroanal. Chem. 587 (2006) 263–268.
[17] S. Miyata, Clay Clay Miner. 31 (1983) 305–311.
[18] S.A. Solin, D. Hines, S.K. Yun, T.J. Pinnavaia, M.F. Thorpe, J. Non-Cryst. Solids 182 (1995) 212–220.
[19] C. Greaves, M.A. Thomas, Acta Crystallogr. B 42 (1986) 51–55.
[20] A. Szytula, A. Murasik, M. Balanda, Phys. Stat. Sol. B 43 (1971) 125–128.
[21] L. Xu, Y.-S. Ding, C.-H. Chen, L. Zhao, C. Rimkus, R. Joesten, S.L. Suib, Chem. Mater. 20 (2007) 308–316.
[22] S. Zhang, H.C. Zeng, Chem. Mater. 21 (2009) 871–883.
[23] Z.-H. Liang, Y.-J. Zhu, X.-L. Hu, J. Phys. Chem. B 108 (2004) 3488–3491.
[24] V. Rives, Layered Double Hydroxides: Present and Future, Nova Science Publishers Inc, New York, 2001.
[25] P. Baraldi, G. Davolio, Mater. Chem. Phys. 21 (1989) 143–154.
[26] M. Rajamathi, P.V. Kamath, R. Seshadri, J. Mater. Chem. 10 (2000) 503–506.
[27] P. Atkins, J. de Paula, Physical Chemistry, 7th ed., Oxford University Press, Oxford, 2002.
[28] J.H. Lee, S.W. Rhee, D.-Y. Jung, Chem. Mater. 16 (2004) 3774–3779.
[29] L. Zhang, F. Li, X. Xiang, M. Wei, D.G. Evans, Chem. Eng. J. 155 (2009) 474–482.
[30] Z.P. Liu, R.Z. Ma, M. Osada, N. Iyi, Y. Ebina, K. Takada, T. Sasaki, J. Am. Chem. Soc. 128 (2006) 4872–4880.
[31] M. Morishita, T. Kakeya, S. Ochiai, T. Ozaki, Y. Kawabe, M. Watada, T. Sakai, J. Power Sources 193 (2009) 871–877.
[32] M. Casas-Cabanas, J. Rodriguez-Carvajal, J. Canales-Vazquez, M.R. Palacin, J. Mater. Chem. 16 (2006) 2925–2939.
[33] K. Watanabe, T. Kikuoka, N. Kumagai, J. Appl. Electrochem. 25 (1995) 219.
[34] D.A. Corrigan, R.M. Bendert, J. Electrochem. Soc. 136 (1989) 723–728.
[35] J. Fan, Y. Yang, Y. Yang, H. Shao, Electrochim. Acta 53 (2007) 1979–1986.
[36] W.Y. Li, S.Y. Zhang, J. Chen, J. Phys. Chem. B 109 (2005) 14025–14032.
[37] X. Mi, X.P. Gao, C.Y. Jiang, M.M. Geng, J. Yan, C.R. Wan, Electrochim. Acta 49 (2004) 3361–3366.
[38] M. Oshitani, M. Watada, K. Shodai, M. Kodama, J. Electrochem. Soc. 148 (2001) A67–A73.
[39] J. Ren, J. Yan, Z. Zhou, X. Wang, X. Gao, Int. J. Hydrogen Energy 31 (2006) 71–76.
[40] Q. Fang, Y. Cheng, X. Jian, L. Zhu, H. Yu, Z. Wang, L. Jiang, J. Rare Earths 28 (2010) 72–78.
[41] T. Moeller, H.E. Kremers, J. Phys. Chem. 48 (1944) 395–406.
[42] W.-H. Zhu, J.-J. Ke, H.-M. Yu, D.-J. Zhang, J. Power Sources 56 (1995) 75–79.